

Article

Eggshell-supported Catalysts for the Advanced Oxidation Treatment of Humic Acid Polluted Wastewaters

Paula Oulego ^{*}, Amanda Laca, Sonia Calvo and Mario Díaz ^{*}

Department of Chemical and Environmental Engineering, University of Oviedo, C/ Julián Clavería, s/n. 33071 Oviedo, Spain; lacaamanda@uniovi.es (A.L.); sonia10_3095@hotmail.com (S.C.)

^{*} Correspondence: oulegopaula@uniovi.es (P.O.); mariodiaz@uniovi.es (M.D.);

Tel.: +34-985-10-34-43 (P.O.); +34-985-10-34-39 (M.D.)

Received: 31 October 2019; Accepted: 25 December 2019; Published: 27 December 2019



Abstract: Metal nanoparticles have been reported as effective catalysts for the removal of refractory compounds from industrial wastewaters in advanced oxidation processes. Additionally, hundreds of thousands of tons of eggshells are discarded worldwide each year. In this work, this waste has been evaluated as support for the synthesis of nanomaterials by wet impregnation method. Four supported catalysts, with a load of iron or copper of 5% and 15%, were prepared and thoroughly characterized by means of different techniques (elemental analysis, XRF, XRD, FTIR, N₂ adsorption-desorption, SEM, TEM and TGA). The catalysts performance was evaluated in wet oxidation tests to degrade humic acids, analyzing the evolution with time of COD, biodegradability index (BOD₅/COD), color number and pH. The best results were achieved with 15% Cu and 5% Fe catalysts (COD reduction being 82.3% and 75.1%, respectively), whereas a COD reduction of 58% was obtained employing non-impregnated eggshell. This can be mainly attributed to the metal loading and the good metal distribution on the surface of the support. The BOD₅ value of humic acids was initially null and, in all assays, the oxidation treatment enhanced the biodegradability. Therefore, eggshell has proved to be an interesting material to be employed as support in nanoparticles preparation.

Keywords: copper-supported catalysts; eggshell; heterogeneous catalysis; humic acid; iron-supported catalysts; nanomaterials; wastewaters; wet oxidation

1. Introduction

Nowadays, one of the main concerns for human society is the absence of clean water [1]. Certainly, two-thirds of the world population might face water stress conditions by 2025, lacking freshwater sources due to water pollution [2]. Industrial processes are responsible for the generation of increasing amounts of wastewaters, contaminated with toxic and hazardous organic compounds, which can cause severe problems into the environment [3]. These wastewaters can be treated by various conventional treatment methods. However, some of them seem to be ineffective for the complete removal of pollutants, especially refractory organic compounds, such as fulvic and humic substances [4,5]. As a major form of humic substances, humic acids (HA) present a very complex chemical structure. HA consist of a heterogeneous association of molecules containing a variety of functional groups, including quinone, aldehyde, carboxyl, phenolic, and alcoholic hydroxyls and other ones, which vary significantly with different sources and origins and behave with a high degree of aromaticity [6]. The presence of HA is a problem in water industry due to their water-soluble formation, wide range of distribution in molecular weight and size, and their non-biodegradability [7]. Additionally, advanced oxidation processes (AOPs), such as wet oxidation (WO) treatments, are gaining increasing interest

due to their ability to degrade refractory organic matter and enhance the biodegradability of the recalcitrant compounds in industrial wastewaters [8,9]. Indeed, WO has been reported as a very attractive technology for the treatment of industrial waste streams that are too dilute to be incinerated and too toxic to be biologically treated [10]. In this context, the use of catalyst in WO process (CWO) is an interesting alternative for the destruction of refractory organic compounds. In fact, CWO has been successfully employed in the treatment of diverse industrial wastewaters (textile, paper, food, chemical, pharmaceutical, and alumina industries) [11]. Additionally, CWO can reduce the severity of the WO conditions. In particular, pressures and temperatures within the ranges of 5–60 bar and 112–320 °C, respectively, can be found in literature for WO processes [12], whereas Heponiemi et al. 2015 [13] indicated that, in CWO treatments, moderate temperatures (between 130 and 200 °C) and 50 bar as maximum pressure were employed.

Different attempts to synthesize heterogeneous catalysts by using solid supports have been carried out. In this sense, one of the methods used for improving the characteristics of a catalyst includes the addition of metal particles to nanomaterials [14,15]). These nanomaterials are commonly employed in many applications of different fields because of their unique characteristics. Specifically, metal nanoparticles can be used as catalysts for the removal of organic compounds [16,17]. The environmental concern has led to the synthesis of heterogeneous base catalysts derived from agro-food wastes, which have been employed as efficient green heterogeneous catalysts [18,19]. These bio-derived materials obtained from wastes have gained great interest due to a growing need to develop green technologies in material synthesis [20]. Eggshell, which is mainly composed of calcium carbonate (CaCO_3) (~94 %wt.), represents approximately 10% of hen egg. Thus, annually, several billion tons of eggshell wastes are produced worldwide, and no significant uses have been found [21,22]. Eggshell waste has been employed as catalyst in different processes, including wastewater treatment. Moreover, this waste has also been used as support for the preparation of catalysts [23] or novel adsorbents [24]. Few works on copper- or iron-impregnated eggshell catalysts have been carried out and, to the best of our knowledge, the use of catalysts derived from eggshell wastes have not been evaluated before in CWO processes.

Therefore, the aim of this work was the assessment of eggshell wastes as an environmentally friendly and economically feasible material to be employed as support for the synthesis of different copper and iron heterogeneous nanocatalysts. These catalysts, and also the eggshell without being impregnated with metal, were thoroughly characterized in terms of chemical composition (elemental analysis and XRF), structure (XRD and FTIR), texture (N_2 adsorption-desorption at 77 K), thermal stability (TGA) and morphology (SEM and TEM). Furthermore, the catalytic activity of these materials was evaluated in WO tests to degrade HA, a refractory compound frequently found in industrial wastewaters. During the treatment, the time evolution of different physicochemical parameters of interest was analyzed: Chemical oxygen demand (COD), biodegradability index (BOD_5/COD), color number (CN), and pH.

It is worthy to note that eggshell can be used as support for the synthesis of heterogeneous catalysts to be used in the catalytic wet oxidation of humic acid. The greatest catalytic activity was obtained with copper (15%wt.) supported on calcined eggshell, thus achieving a COD removal of 82.3% after 6 h of WO. A homogeneous metal distribution on the surface of eggshell and a high metal loading is essential to achieve a high degradation removal.

2. Materials and Methods

2.1. Reagents

$\text{Fe}(\text{NO}_3)_3 \cdot 9\text{H}_2\text{O}$ ($\geq 98\%$), $\text{Cu}(\text{NO}_3)_2 \cdot 3\text{H}_2\text{O}$ (puriss. p.a., 99–104%), Ag_2SO_4 ($\geq 99.5\%$), H_2SO_4 (95–98%), HgSO_4 ($\geq 99\%$), $\text{K}_2\text{Cr}_2\text{O}_7$ ($\geq 99\%$), $\text{MgSO}_4 \cdot 7\text{H}_2\text{O}$ ($\geq 98\%$), $\text{CaCl}_2 \cdot 2\text{H}_2\text{O}$ ($\geq 99\%$), NH_4Cl ($\geq 99.5\%$), $\text{FeCl}_3 \cdot 6\text{H}_2\text{O}$ (puriss. p.a., $\geq 99\%$), KH_2PO_4 ($\geq 98\%$), K_2HPO_4 ($\geq 98\%$), and humic acid (technical grade) were supplied by Sigma-Aldrich. Hen eggs were purchased from a local supermarket.

2.2. Preparation of the Catalysts

Shelling of the eggs were performed manually, yolk and albumen were discarded and shell membranes were removed using tweezers. Eggshells were rinsed several times with deionized water and they were left to air dry for 8 h at 105 °C. The dried eggshells were crushed and ground into small pieces (<2 mm) using a grinder and, then, they were calcined for 12 h at 700 °C. Next, they were sieved through 355 µm and the powder obtained was dried again for 8 h at 105 °C.

The iron and copper supported catalysts were prepared by wet impregnation [25]. In the case of 5%wt. CuO/calcined eggshell, 10 g of calcined eggshell was added to a solution of $\text{Cu}(\text{NO}_3)_2 \cdot 3\text{H}_2\text{O}$ (1.92 g, 7.95 mmol) in 30 mL of water stirred for 1 h at room temperature. The liquid was evaporated overnight on a silicon oil bath at 70 °C, obtaining a light blue powder. This was dried at 105 °C for 8 h and then calcined in air at 300 °C (2.5 °C/min) for 4 h. For the synthesis of 15%wt. CuO/calcined eggshell, the same procedure was followed, although in the case 5.76 g (23.84 mmol) of $\text{Cu}(\text{NO}_3)_2 \cdot 3\text{H}_2\text{O}$ was added. The same methodology was used for the preparation of 5%wt. Fe_2O_3 /calcined eggshell and 15%wt. Fe_2O_3 /calcined eggshell. In these syntheses, 3.69 g (9.13 mmol) of $\text{Fe}(\text{NO}_3)_3 \cdot 9\text{H}_2\text{O}$ and 11.07 g (27.40 mmol), respectively, were added.

2.3. Techniques of Characterization

A PerkinElmer 2400 analyzer (PerkinElmer, Inc., Waltham, MA, USA) with a Perkin Elmer AD-2Z microbalance was used for the elemental analysis. A Shimadzu EDX-720 energy dispersive X-Ray fluorescence (XRF) spectrometer (Shimadzu Corporation, Kyoto, Japan) was used to determine the chemical composition of the iron and copper-based nanomaterials. Powder X-ray diffraction (XRD) patterns were obtained with a PANalytical X'Pert Pro powder diffractometer (Malvern Panalytical, Malvern, Worcestershire, UK) employing $\text{Cu K}\alpha$ radiation ($\lambda_{\text{K}\alpha} = 1.5406 \text{ \AA}$) and a graphite secondary monochromator. Diffractograms were recorded for 2θ values between 10° and 80° by a 0.02° step, with a scan step time of 1 s. The Malvern Panalytical's HighScore software by PANalytical was employed for the analysis of the XRD spectra [26].

FTIR analysis were carried out using a Varian 670-IR spectrometer (Agilent Technologies, Inc., Santa Clara, CA, USA). The attenuated total reflectance (ATR) accessory was mounted in the sample compartment. Spectra were acquired in the mid-IR region from 4000 to 600 cm^{-1} and signals were collected in 16 scans at a resolution of 4 cm^{-1} .

In order to determine the specific surface area and porous structure of the materials, a Micromeritics ASAP 2020 instrument (Micromeritics Instrument Corporation, Norcross, GA, USA) was used to perform N_2 adsorption-desorption tests at 77 K. Before the analysis, it was necessary to degas the samples at 120 °C for 10 h. Analysis of mesoporosity was performed through the BJH method [27]. The MicroActive data analysis software (V4.03) by Micromeritics was used for the analysis of the textural data.

The microscopic morphology of the samples was performed using a JEOL JMS-6610LV (JEOL Ltd., Kyoto, Japan) scanning electron microscope (SEM) operating at 0.3–30 kV. Prior to the SEM analyses, the catalysts were sputter-coated with a thin layer of gold.

Transmission electron microscopy (TEM) was performed on a MET JEOL-2000 EX-II (JEOL Ltd., Kyoto, Japan) microscope with an operating voltage of 200 kV. High angle annular dark-field scanning TEM (HAADF-STEM) and energy-dispersive X-ray (EDX) analysis were carried out on a MET JEOL-JEM 2100F microscope (JEOL Ltd., Kyoto, Japan) with an operating voltage of 200 kV. Before the analyses, the catalysts were dispersed into ethanol, sonicated for 2 min and dropped onto carbonated copper grids.

TGA analysis of the samples were performed with a Mettler Toledo TGA/STDA851e instrument (Mettler Toledo, Columbus, OH, USA), under an oxygen atmosphere, the gas flow rate being 50 mL/min. The temperature was increased from 25 to 1000 °C, at a heating rate of 10 °C/min.

2.4. Catalytic Experiments (WO): Apparatus and Procedure

The catalytic tests were carried out in a 1 L semi-batch reactor (Parr T316SS) (Parr Instrument Company, Moline, IL, USA) equipped with two six-bladed magnetically driven turbine agitators and a rupture disc to prevent the pressure from exceeding 120 bar. Besides the reactor, the experimental setup was composed of temperature, pressure and air flow controllers with the corresponding indicators, a heating blanket and a sampling system. Specifically, pressure was adjusted by a back-pressure control valve located at the gas outlet. Finally, a 2 L stainless steel water reservoir preceded the reactor in order to saturate the air flow, which was provided by a compressed bottle. The loaded volume in each vessel was about 70% of the total to ensure safe operating conditions. The procedure is described more detailed by Oulego et al. [28].

Temperature chosen for the experiment was 150 °C, whereas pressure was maintained constant at 40 bar. These conditions were selected based on our studies related to the WO of landfill leachates, which contain HA in their composition [8,28]. The stirring speed and the oxygen flow rate were adjusted to 400 rpm and 1800 mL/min, respectively. In a typical experiment, 0.7 L of synthetic water, i.e., a solution of 400 ppm of HA and the catalyst (0.7 g) were introduced into the reaction vessel, then the reactor was pressurized and heated up to the desired conditions, which were maintained constant during the course of each experiment (6 h). The concentration of HA was selected because it is within the range considered by other authors (from 2.5 mg/L to 3.3 g/L) during the treatment of HA using oxidation processes [29,30]. Throughout the experiment, samples were periodically taken and analyzed and the catalysts were removed by filtration using hydrophilic PVDF membrane with 0.22 µm of pore size. Synthetic water was prepared adding some pellets of NaOH to obtain a basic pH to achieve the total dissolution of HA, once the HA was dissolved the pH was adjusted to 7.5 employing H₂SO₄ 5 M.

The experiments were carried out at least in duplicate and as separate, independent experiments. The reproducibility was high in all cases, the standard deviation being 10% as maximum.

2.5. Catalytic Experiments: Sample Analysis

The pH was measured employing a Basic 20 Crison pH-meter (Crison Instruments, S.A., Alella, Barcelona, Spain). The color number (CN) was calculated by measuring the absorbance at three wavelengths (436 nm, 525 nm and 620 nm) using a spectrophotometer SPEKOL 1500 (Analytik Jena, A.G., Jena, Germany). The Equation (1) was applied [28]:

$$\text{CN} = \frac{\text{ABS}_{436}^2 + \text{ABS}_{525}^2 + \text{ABS}_{620}^2}{\text{ABS}_{436} + \text{ABS}_{525} + \text{ABS}_{620}} \quad (1)$$

Where, ABS_i is the value of the absorbance at the specific wavelength i.

The concentration of organic load was determined by means of chemical oxygen demand (COD) using the dichromate method. This parameter was measured according to the Standard Methods [31]. Briefly, 3 mL of the aqueous solution after WO treatment, 2 mL of a digesting solution (solution D) and 3 mL of an acidic solution (solution A) were introduced in a digestion tube. Afterwards, the blend was mixed and digested in a COD reactor (Hach) for 2 h at 150 °C. Once the sample is cold, COD was spectrophotometrically determined at 600 nm in a DR2500 spectrophotometer (Hach, Loveland, CO, USA). The solution A was prepared by mixing 6.6 g of Ag₂SO₄ in 1 L of concentrated H₂SO₄ (98%). The solution D was prepared by mixing 20 g of HgSO₄ in 500 mL of K₂Cr₂O₇ 0.25 N and 175 mL of solution A.

Biochemical oxygen demand (BOD₅) was measured using a manometric respirometric measurement system, BOD-System OxiDirect[®] (Thermo Fisher Scientific, Hampton, NH, USA). The samples were filtered, using a hydrophilic PVDF membrane with 0.22 µm of pore size, in order to remove the catalysts. The pH was adjusted to 6.5–7.5 with HCl 2.5 M employing a Crison Basic 20 pH-meter. 94 mL of each sample solution were used in the BOD₅ determination. It was necessary to

inoculate the samples with 1 mL of the effluent of an aerobic reactor from a wastewater treatment plant (WWTP) since they were treated by WO and no microorganisms were present. After a mixing step, the inoculated solutions were poured into the BOD bottles and 3 drops of a solution that inhibited the nitrification process were added. Then, they were incubated at 20 °C for 5 days (dark conditions). An aqueous solution composed of MgSO₄ (22.5 mg/L), CaCl₂ (27.5 mg/L), NH₄Cl (1.7 mg/L), FeCl₃·6H₂O (0.25 mg/L), and a phosphate buffer with a pH value of 7.3 (8.5 mg/L of KH₂PO₄ and 21.75 mg/L of K₂HPO₄), and inoculated with 1 mL of the WWTP effluent, was used as a blank sample. The BOD₅ value of the blank sample was deducted from the BOD₅ values of the samples after WO in order not to consider the one due to the inoculum.

The iron and copper content in the aqueous solution after WO was determined by ICP mass spectrometry (ICP-MS), using an Agilent 7700x spectrometer (Agilent Technologies, Inc., Santa Clara, CA, USA). Scandium (⁴⁵Sc) was used as internal standard. Collision cell was employed, the flow rate of He being 4.3 mL/min. The instrumental parameters for ICP-MS are shown in the Supplementary Material (Table S1).

All analytical measurements were carried out at least in triplicate. The reproducibility was high in all cases, the standard deviation being 5% as maximum.

3. Results and Discussion

3.1. Chemical Composition

The elemental analysis of the iron and copper nanomaterials supported on eggshell, named as Fe 5% and Fe 15%, and Cu 5% and Cu 15%, respectively, is shown in Table 1. All catalysts present a significant content of nitrogen, from 2.9% to 7%, approximately, which is due to the use of nitrate precursors in their synthesis. Besides, a little increase in carbon content was also observed in the nanomaterials. This can be due to a slight carbonation of the support, since this phenomenon can be found in calcium compounds, such as eggshell.

Table 1. Elemental analysis of the calcined eggshell and the iron and copper supported nanomaterials.

Sample	% N	% C	% S	% H
Eggshell	0.42 ± 0.05	1.12 ± 0.03	0.25 ± 0.06	1.63 ± 0.04
Fe 5%	2.90 ± 0.06	2.79 ± 0.04	0.27 ± 0.04	1.65 ± 0.07
Fe 15%	6.99 ± 0.07	2.23 ± 0.05	0.25 ± 0.05	1.21 ± 0.08
Cu 5%	1.66 ± 0.04	2.28 ± 0.03	0.25 ± 0.02	1.46 ± 0.08
Cu 15%	4.61 ± 0.07	2.48 ± 0.06	0.27 ± 0.03	1.65 ± 0.06

The chemical composition of the catalysts determined by XRF can be found in Table 2.

Table 2. Chemical composition in weight percentage of the calcined eggshell and the iron and copper supported nanomaterials measured by XRF.

Element	Eggshell	Fe 5%	Fe 15%	Cu 5%	Cu 15%
Ca	98.48 ± 0.04	92.93 ± 0.04	83.81 ± 0.05	93.37 ± 0.05	83.80 ± 0.02
Mg	0.92 ± 0.07	0.85 ± 0.03	0.68 ± 0.03	0.88 ± 0.03	0.70 ± 0.04
Na	0.25 ± 0.03	0.33 ± 0.04	0.25 ± 0.02	0.29 ± 0.04	0.28 ± 0.03
P	0.29 ± 0.03	0.27 ± 0.02	0.23 ± 0.02	0.26 ± 0.03	0.27 ± 0.04
K	0.05 ± 0.01	0.06 ± 0.01	0.06 ± 0.01	0.05 ± 0.02	0.05 ± 0.02
Fe	n.d. *	5.42 ± 0.01	14.96 ± 0.06	n.d. *	n.d. *
Cu	n.d. *	n.d. *	n.d. *	5.14 ± 0.05	14.89 ± 0.09

* n.d.: not detected.

As expected, the main component was Ca. Besides, Mg was present in low concentration, and P, Na, and K were identified as trace elements. These analyses also allowed us to prove that both iron and copper supported catalysts were synthesized appropriately. In this sense, the weight percentage of iron was $5.42 \pm 0.03\%$ and $14.96 \pm 0.06\%$, and the one of copper was $5.14 \pm 0.05\%$ and $14.89 \pm 0.09\%$, for the catalysts prepared with a theoretical load of iron or copper of 5% and 15%, respectively.

3.2. Structural Characterization: XRD and FTIR Analyses

XRD analyses were carried out in order to obtain the crystalline structure of the catalysts. The diffraction patterns of the support (calcined eggshell) and the iron and copper catalysts are depicted in Figure 1.

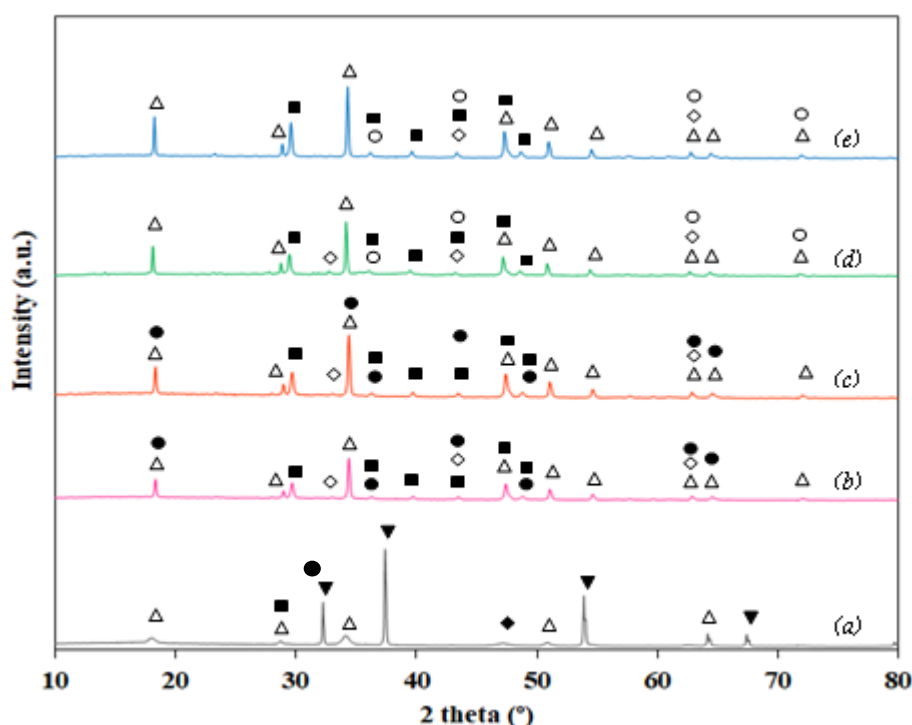


Figure 1. XRD patterns between 10° and 80° of (a) calcined eggshell, (b) Fe 5%, (c) Fe 15%, (d) Cu 5%, and (e) Cu 15%. Symbols: $\text{Ca}(\text{OH})_2$ (Δ), CaCO_3 (\blacksquare), CaO (\blacktriangledown), MgCO_3 (\blacklozenge), MgO (\diamond), Fe_2O_3 (\bullet), and CuO (\circ).

The diffractogram of the calcined eggshell (Figure 1a) shows that the support is made up of calcium oxide (CaO) and calcium hydroxide ($\text{Ca}(\text{OH})_2$). In this sense, three sharp peaks, which are indicative of the existence of an important level of crystallinity, were identified. These peaks at 32.2° (111), 37.4° (200), 53.8° (220) and a low intense one at 67.4° (222) can be assigned to CaO [32,33]. This is due to the thermal decomposition of CaCO_3 to CaO caused by its calcination at 700°C . Small peaks detected at 28.7° (104) and 46.8° (202), indicated the presence of calcium carbonate (CaCO_3) and magnesium carbonate (MgCO_3), respectively, as impurities. Besides, characteristic peaks of $\text{Ca}(\text{OH})_2$ at 18.1° (001), 28.7° (100), 33.9° (011), 51.3° (110), and 64.5° (103) were also observed [32,33].

For both iron and copper supported catalysts, CaO was not identified. However, characteristic peaks of CaCO_3 were distinguished at 29.3° (104), 35.9° (110), 39.4° (113), 43.1° (202), 47.4° (018), and 48.5° (116). Therefore, the calcination at 300°C for 4 h was not enough to properly decompose CaCO_3 into CaO . Moreover, it was observed characteristic peaks of $\text{Ca}(\text{OH})_2$ at the same positions as those found for the calcined eggshell and at new ones: 47.1° (102), 54.3° (111), 62.6° (201), and 71.8° (202) [33]. Magnesium oxide was also detected as impurity, since some characteristics peaks of this

compound at 37.8° (111), 43.1° (200) overlapped with CaCO_3 , and at 62.6° (220) overlapped with $\text{Ca}(\text{OH})_2$, were identified [34].

Besides, in the case of the iron supported catalysts, peaks at 18.1° (111), 33.9° (310), 35.6° (311), 43.1° (400), 48.5° (420), 62.6° (440), and 64.5° (530), which were attributed to maghemite ($\gamma\text{-Fe}_2\text{O}_3$), were identified [35]. It should be noted that these peaks are overlapped with the ones of $\text{Ca}(\text{OH})_2$ or CaCO_3 .

For the copper supported catalysts, it was distinguished characteristic peaks of CuO at 37° (111), 43.0° (200), 62.4° (220), and 71.8° (311) [36]. Some of these peaks were also overlapped with those found in $\text{Ca}(\text{OH})_2$ or CaCO_3 .

The FTIR spectra of the catalysts from 4000 to 600 cm^{-1} are shown in Figure 2.

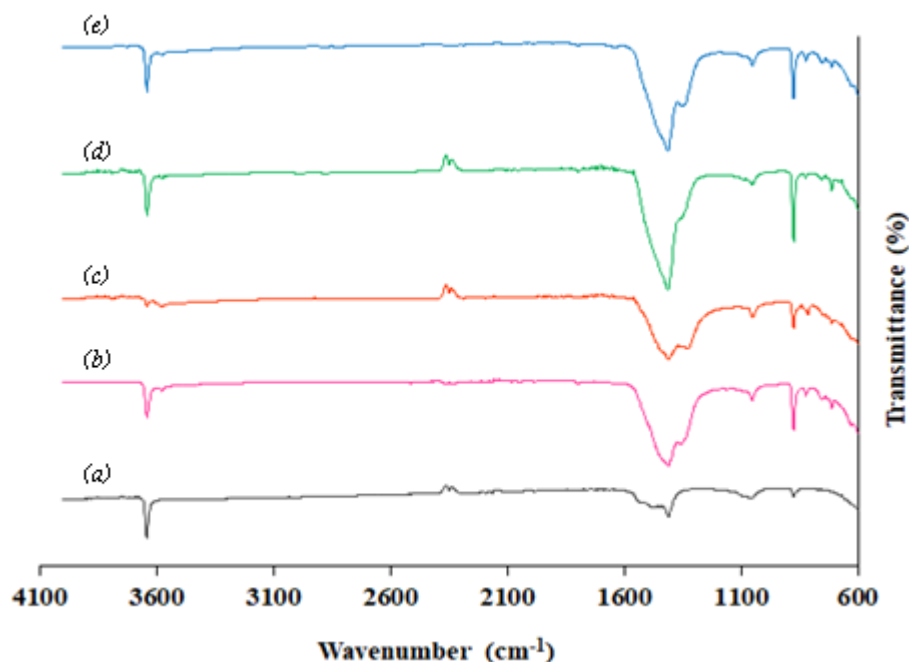


Figure 2. FTIR spectra from 4000 to 600 cm^{-1} of (a) calcined eggshell, (b) Fe 5%, (c) Fe 15%, (d) Cu 5%, and (e) Cu 15%.

For both calcined eggshell and the supported catalysts, the major absorption band identified at 1409 cm^{-1} was attributed to the asymmetric stretch of CO_3^{2-} [33,37]. It was also observed a sharp peak at 873 cm^{-1} due to the out-of-plane bending vibration of CO_3^{2-} [33,37]. A small peak that appeared at 1049 cm^{-1} is from bulk mode (physical mixture) [28]. Besides, it was distinguished a sharp peak at 3639 cm^{-1} , which can be assigned to the OH stretching vibration of $\text{Ca}(\text{OH})_2$ [33].

In the case of the iron and copper catalysts, a very low intense peak at 3573 cm^{-1} , due to the OH stretching vibration from moisture water, was detected. This can be explained by considering the hygroscopic nature of eggshell according to Mosaddegh et al. [38]. A small shoulder at around 1350 cm^{-1} , which can be attributed to the stretching vibration of NO_3^- , was observed [39]. This is due to the nitrate precursors used in the synthesis. Besides, it was identified a peak at 711 cm^{-1} , which can be due to the Ca-O bond and in-of-plane bending vibration of CO_3^{2-} [40,41]. For the iron supported catalysts, small bands at around 800 , 730 , and 625 cm^{-1} was due to maghemite vibrations [39,42]. It should be noted that the band at 730 cm^{-1} is overlapped with the stretching vibration of Ca-O group [43]. Considering the copper supported catalysts, a low intense band at 610 cm^{-1} assigned to the Cu-O stretching vibration was identified [44]. These results are in agreement with those obtained in the XRD measurements.

3.3. Textural Characterization

N₂ adsorption-desorption isotherms of the calcined eggshell and the supported catalysts are shown in Figure S1 of the Supplementary Material. Based on the International Union of Pure and Applied Chemist (IUPAC) classification, the isotherms obtained are consistent with type IIa, which is characteristic of macroporous solids [45].

Table S2 summarizes the textural parameters of the calcined eggshell and the catalysts. Specific surface areas were calculated using the Brunauer–Emmett–Teller (BET) method. The average values of pore diameter were, in general, superior to 50 nm, thus indicating their macroporous nature, in accordance with the isotherm observed. It should be noted that the specific surface area (BET area) and pore volume of the calcined eggshell (4 m²/g and 0.059 cm³/g, respectively) were similar to those reported for other authors, who used a calcination temperature of 600 °C [46]. Regarding the supported catalysts, in all cases, wet impregnation caused an increase in both BET area (~1.5 times higher) and pore volume (from 1.5 to 3 times higher), except for the Fe 15% catalyst, in which the BET area was half the value obtained for the calcined eggshell.

3.4. Microstructure: SEM and TEM microscopy

SEM micrographs of the support and the catalysts can be found in Figure 3. On viewing these figures, it should be noted that the calcined eggshell is made up of pseudo cubic particles, the average size being 385 nm.

It is worthy to note that interparticle cavities were observed in both the support and the catalysts, which could explain their macroporosity character (Figure 3a).

For the iron and copper supported catalysts, the cubic-like structure is not well defined as in the case of the eggshell. In this sense, the impregnation caused a modification in their microstructure, leading to the formation of a mixture of particle aggregates with different shapes and sizes. Hence, particles with an average length of 550 nm and width of 215 nm were identified in the Cu 5% catalyst, while in the Cu 15% one, the sizes were a bit lower, the length and width being 328 nm and 80 nm, respectively.

Moreover, the catalysts presented an uneven surface due to the metal impregnation. Likewise, it is possible to distinguish a slight increase in the porous structure. It is considered that the zones of the micrographs smoother and less colored are the ones in which there is no presence of either iron or copper, thus identifying the impregnated metals as darker spots (Figure 3b). This was proved performing HAADF-STEM analysis. The results can be found in Figures S3–S6 of the Supplementary Material.

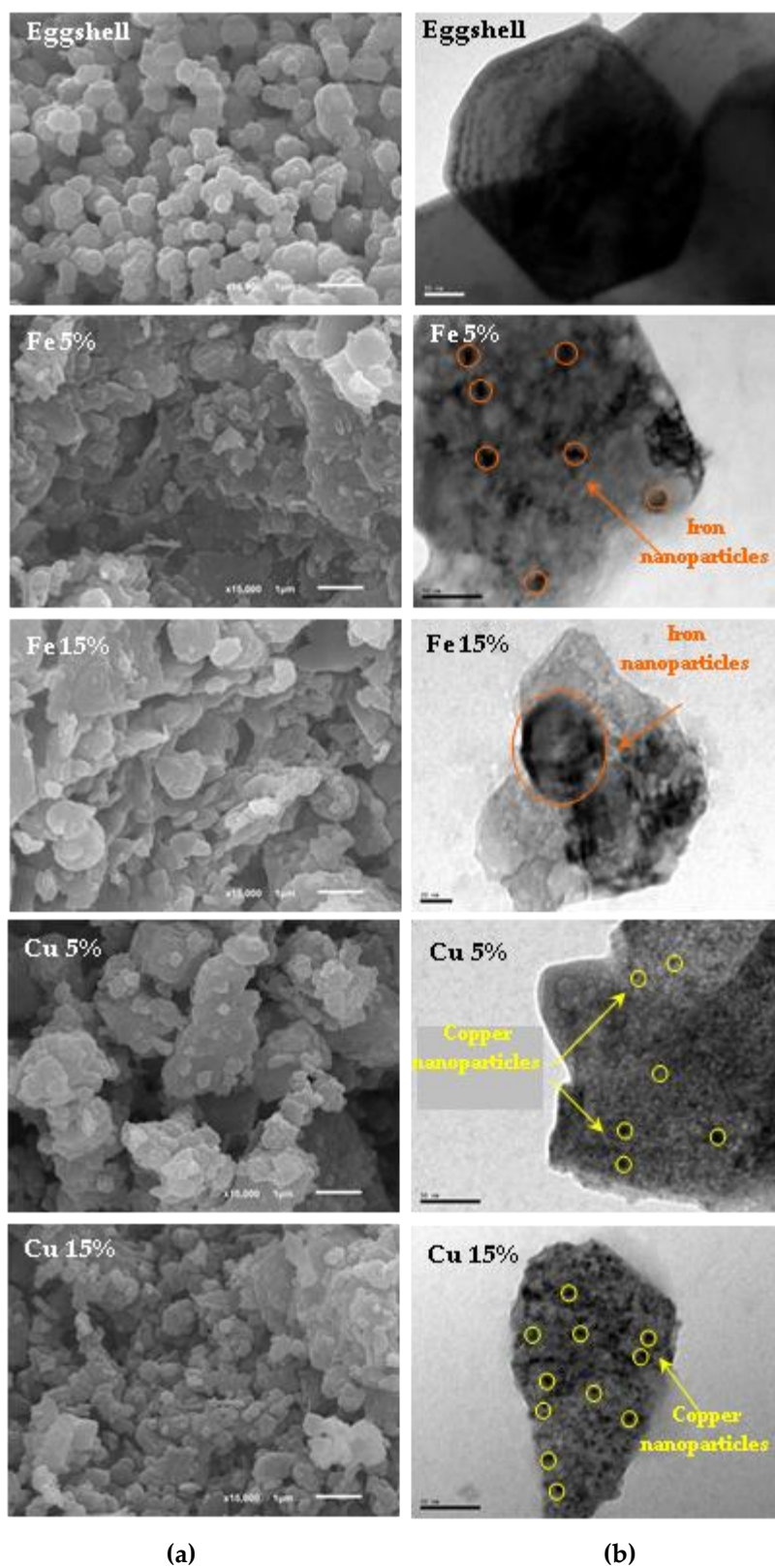


Figure 3. (a) SEM images and (b) TEM images of the calcined eggshell and the iron and copper supported catalysts.

3.5. Thermal Stability

The thermal stability of the calcined eggshell and the supported catalysts was determined by means of thermogravimetric analyses (TGA) from room temperature to 1000 °C. TGA results can be found in Figure 4, in which TG is the percentage of weight loss and DTG is the derivative of weight loss.

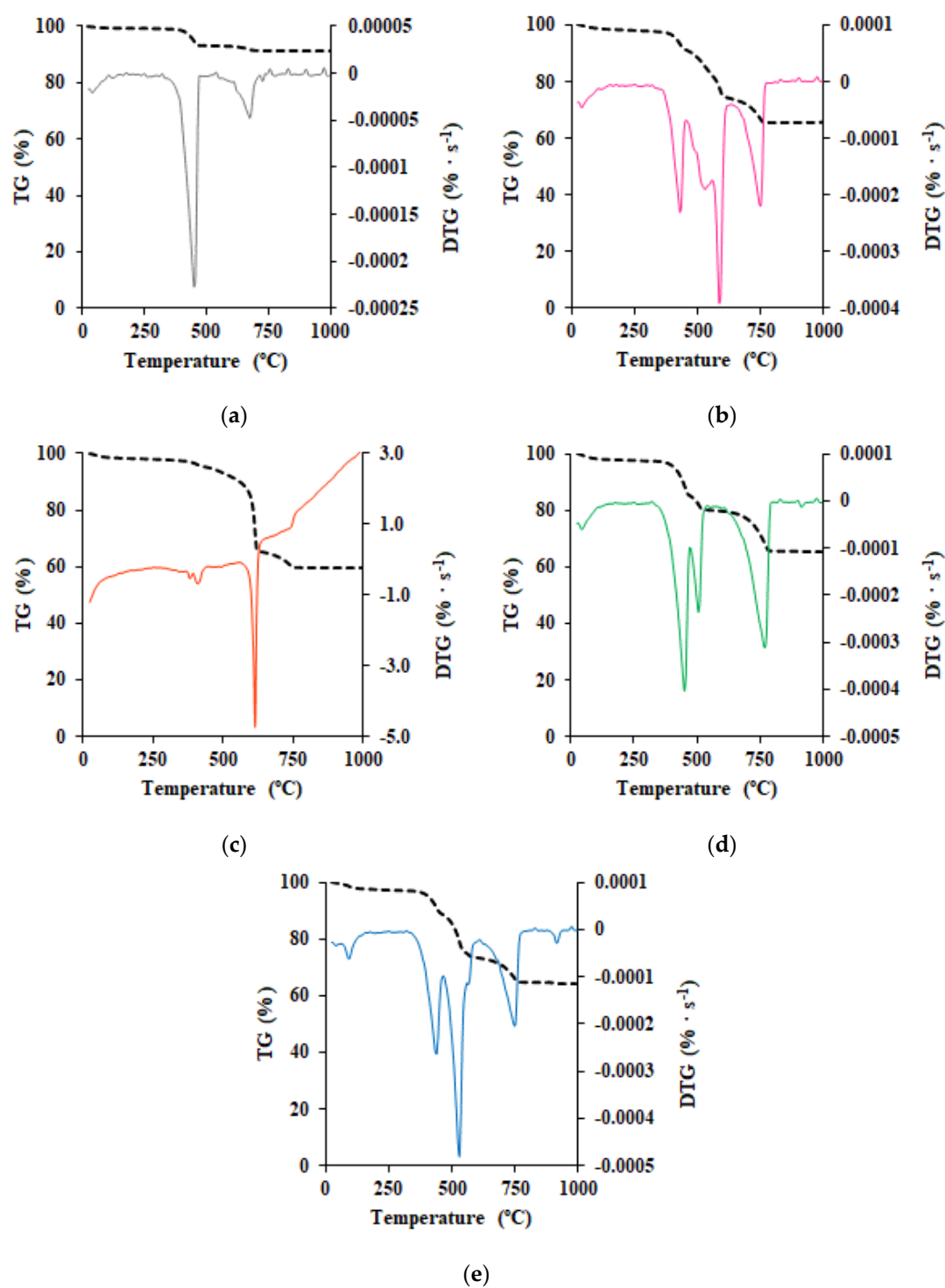


Figure 4. TG (percentage of weight loss) and DTG (derivative of weight loss) curves in an oxygen atmosphere at a heating rate of 10 °C/min: (a) calcined eggshell, (b) Fe 5%, (c) Fe 15%, (d) Cu 5%, and (e) Cu 15%.

On viewing the results, both the support and the catalysts presented a high thermal stability under oxidative atmosphere. Hence, the onset decomposition temperatures were above 350 °C, the values varying between 380 °C and 400 °C. Regarding the calcined eggshell, TG curve shows three stages of weight loss as temperature increases. The first one, from 25 °C to 105 °C, in which the loss is minimum (0.5%). This is due to the evaporation of water molecules from its surface. The second one, from 105 °C to 510 °C, is attributed to the transformation of $\text{Ca}(\text{OH})_2$ to CaO [47]. At this stage, the weight loss was maximum (6.2%) according to the DTG curve. The third one, between 510 °C and 745 °C, can be assigned to the transformation of CaCO_3 to CO_2 , the value of weight loss being 1.8% [33]. Further heating above 745 °C did not cause any effect to the sample, remaining around 91% of the initial sample.

Considering the iron and copper supported catalysts, three stages of weight loss were also observed based on the TG curves. Firstly, between 25 °C and 125 °C, a low loss (1.8%), which is attributed to the moisture water because of the hygroscopic nature of eggshell, was observed [38]. Secondly, from 125 °C to 600–635 °C, in which the weight loss achieved the highest value (from 18.6% to 29.4%) as indicated the DTG curves. Two weight losses were identified: i) in the range of 125 °C to 460–470 °C, which can be assigned to the transformation of $\text{Ca}(\text{OH})_2$ to CaO and ii) in the range of 460–470 °C to 600–635 °C, which is due to the decomposition of copper and iron nitrate precursors [48]. Thirdly, from 600–635 °C to 800 °C, with an average weight loss of 8.5%. This stage can be attributed to the decomposition of CaCO_3 [49].

In the same way as with the calcined eggshell, heating above 800 °C did not cause any effect to the materials. However, it should be noted that the total weight loss of the calcined eggshell was around 4 times lower than those obtained for the catalysts (between 34.1 and 40.5%).

On viewing these results, there are practically no changes in the catalysts and support at the temperature employed in the wet oxidation tests (150 °C), thus indicating that these materials are stable at the working conditions.

3.6. Catalytic Properties

WO tests were carried out for 6 h using the calcined eggshell and the iron and copper nanoparticles as catalysts. Additionally, WO of synthetic water in absence of catalyst was performed in order to evaluate the effect of the different materials employed in the treatment.

The evolution of COD concentration during the wet oxidation of HA is shown in Figure 5.

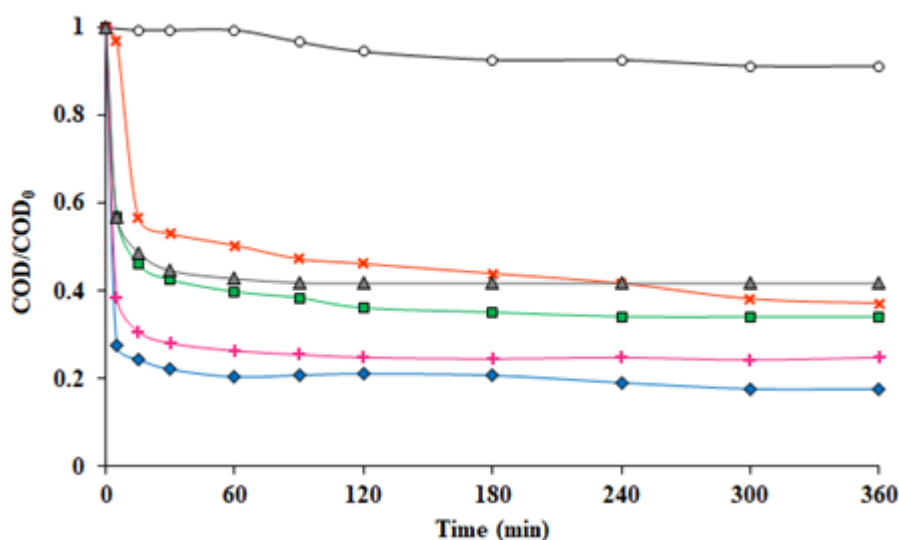


Figure 5. Evolution of chemical oxygen demand (COD) concentration with time in absence of catalyst (○), and in presence of the eggshell (▲) and the supported catalysts: Fe 5% (+), Fe 15% (×), Cu 5% (■) and Cu 15% (◆). In all cases, $T = 150$ °C, $P = 40$ bar, $\text{pH} = 7.5$, initial COD concentration = 367 ppm and catalyst concentration = 1 g/L.

On viewing the results obtained, the presence of the iron and copper supported catalysts significantly enhanced the removal of organic load, the improvement being more marked at the beginning of the oxidation (first 1 h). In absence of catalyst, after 6 h of wet oxidation, COD removal of 8.8% was attained, thus showing the refractory nature of this pollutant. Nevertheless, when the catalysts were added, removals from 62.8% to 82.3% at the same reaction time, were obtained. The best catalytic results were obtained when the sample Cu 15% was used, achieving a COD removal of 74.1% after 3 h of oxidation. Wang et al. [50] obtained removals of humic substances lower than those reported in this work (60.4%), when they were treated by catalytic WO at 150 °C, 0.5 MPa for 4 h in presence of NaNO₂ as catalyst and promoted by trichlorophenol.

The results here obtained proved the good catalytic behavior of both iron (5%wt.) and copper (15%wt.) supported catalysts for the degradation of HA by catalytic wet oxidation. The catalytic activity of the different solids tested followed this order: Cu 15% > Fe 5% > Cu 5% > Fe 15%. Hence, the greatest activity is the result of a high metal loading and a good distribution of the metal nanoparticles on the surface of the support. This is in agreement with the results reported by other authors [51], in which the catalytic activity of ZSM-5 zeolite to convert methanol to olefins and aromatics was also affected by the metal loading.

ICP-MS analyses were also performed in the samples collected at 15, 180, and 360 min in order to evaluate the leaching of iron and copper during the catalytic WO of HA. The results obtained are shown in Table S3 of the Supplementary Material. It should be noted that iron leaching is practically negligible. In this sense, the highest value (145 µg/L) was achieved after 360 min of WO when Fe 15% was used as catalyst. In the case of copper, its leaching can be considered very low, the highest value being around 450 µg/L (observed after 360 min of WO in presence of Cu 15% as catalyst). Therefore, both catalysts showed good stability throughout the WO treatment.

These results are in agreement with those obtained by XRF, in which the iron content of the used catalysts remained practically constant and the copper one decreased very slightly during the WO treatment (Table S4). This also proved the great stability of the iron and copper supported catalysts.

Besides, the support was also tested for the HA degradation, achieving a COD removal of 58% after 6 h of WO treatment. Therefore, the impregnation of metal nanoparticles under certain conditions led to a significant enhancement in the organic load removal.

The influence of a high pH value (12) on the degradation of HA in absence of catalyst (using pure CaO) was also evaluated. The results obtained indicated that an increase in the pH value had a negative effect on the COD removal (see Figure S2 of the Supplementary Material). In this sense, a removal of 38% was achieved after 6 h of wet oxidation at pH 12, whereas at the same reaction time, the removal was around 1.5 times higher when a pH value of 7.5 was used.

The results related to the biodegradability index, BOD₅/COD, are shown in Figure 6. Due to the refractory nature of HA, the value of BOD₅ of the synthetic water polluted with HA was null. It is worthy to note that the use of calcined eggshell and Fe 15% as catalyst notably enhanced this parameter, achieving a highly biodegradable effluent after the WO treatment (BOD₅/COD > 0.4). Hence, the best results were obtained with the calcined eggshell, with a BOD₅/COD value of 0.73. Moderate biodegradability was obtained when HA solution was treated without catalyst and in presence of the catalyst Cu 5% (BOD₅/COD values from 0.2 to 0.3). The water treated with Cu 15% and Fe15% as catalysts led to low biodegradable effluents, the values of BOD₅/COD being around 0.1. In this sense, a future direction should include the study of the oxidation mechanisms in order to identify the intermediates or final products responsible for the low or high biodegradable values.

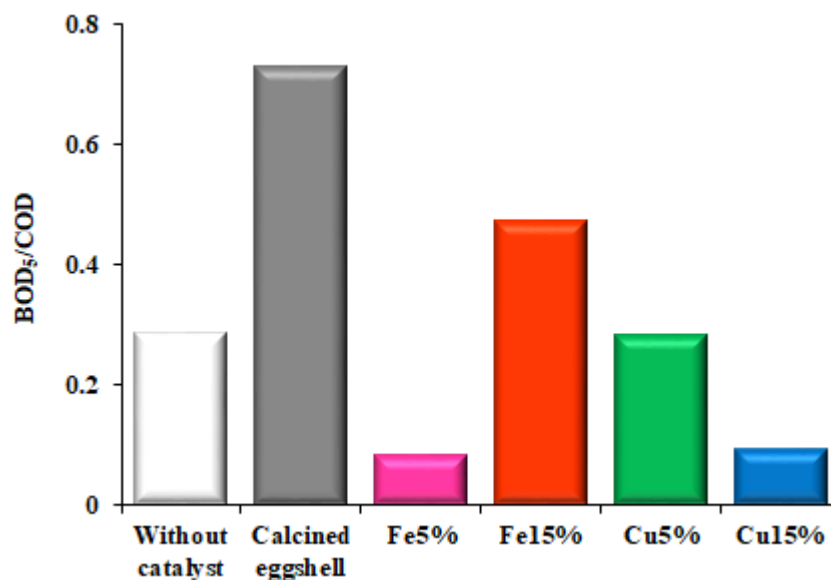


Figure 6. Biodegradability index values after 6 h of wet oxidation in absence of catalyst (□), and in presence of the eggshell (■) and the supported catalysts: Fe 5% (■), Fe 15% (■), Cu 5% (■), and Cu 15% (■). In all cases, T = 150 °C, P = 40 bar, pH = 7.5, initial HA concentration = 400 ppm and catalyst concentration = 1 g/L.

The evolution of the CN values during the wet oxidation treatment can be found in Figure 7. It can be observed that the use of each of the supported catalysts significantly reduced the CN values, obtaining almost a colorless effluent in the first minutes of the reaction, whereas in absence of catalyst, it was necessary around 90 min to achieve a notable removal of color (approximately 80% of reduction in CN). These results highlight the need of employing a catalyst during the oxidation treatment. It has been previously described the ability of WO to reduce color on different wastewaters, as well as the generation of highly colored intermediates during the oxidation of phenol-like compounds [52]. However, in the experiments carried out in the present work, an increase in the CN during the treatment was not observed in any case.

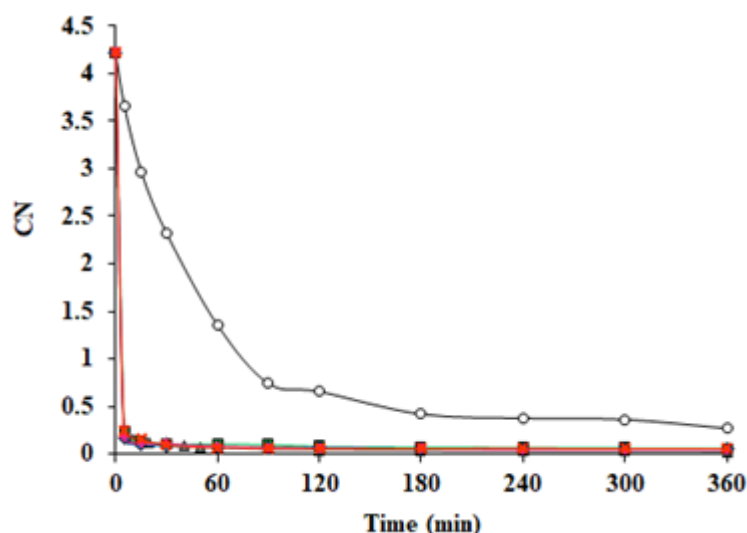


Figure 7. Evolution of color number (CN) values with time in absence of catalyst (○), and in presence of the eggshell (▲) and the supported catalysts: Fe 5% (+), Fe 15% (×), Cu 5% (■), and Cu 15% (◆). In all cases, T = 150 °C, P = 40 bar, pH = 7.5, initial HA concentration = 400 ppm and catalyst concentration = 1 g/L.

Humic acids are characterized by their dark color (from brown to black), which is related to the presence of polycyclic aromatic hydrocarbons. These aromatic compounds present a strong absorbance at 254 nm. Therefore, the evolution of the absorbance at this wavelength during the WO treatment was determined (Figure 8).

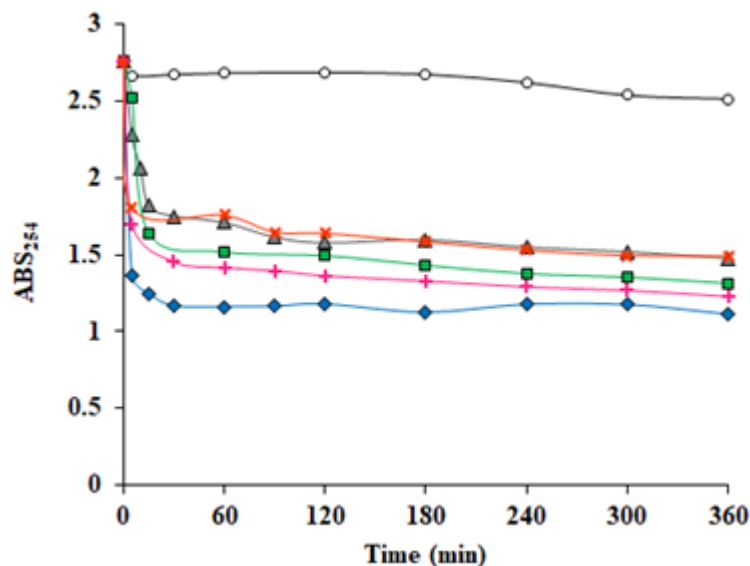


Figure 8. Evolution of ABS_{254} values with time in absence of catalyst (○), in presence of the eggshell (△) and the supported catalysts: Fe 5% (+), Fe 15% (×), Cu 5% (■), and Cu 15% (◆). In all cases, $T = 150\text{ }^{\circ}\text{C}$, $P = 40\text{ bar}$, $\text{pH} = 7.5$, initial HA concentration = 400 ppm and catalyst concentration = 1 g/L.

The degradation of humic substances in terms of ABS_{254} absorbance using advanced oxidation processes was also studied by Mahvi et al. [29], who found that the degradation efficiency of humic substances reached a maximum value of 9.5% after 300 min of ultrasonolysis. Here, a similar value of degradation was achieved when the synthetic water was treated without catalyst, whereas much higher values were obtained when catalysts were employed during the WO process, the values ranging from 46.4% to 59.6%. The poor effects of ultrasonic degradation on the reduction efficiency of ABS_{254} can be due to the fact that low ultrasound frequencies hinder the development of hydroxyl radicals [29]. This can also be the reason to explain the results obtained here, since hydroxyl radicals are known to be reactive and non-selective species, which are involved in the chemistry of many advanced oxidation processes for the degradation of organic compounds. In addition, unsaturated groups, such as aromatic ones, are converted into saturated groups and ring-opening products via the attack of hydroxyl radicals, which may lead to a decrease in absorptivity at 254 nm [53]. Thus, the best results were achieved in the presence of catalysts, since metals enhance the generation of highly reactive hydroxyl radicals [54,55].

The evolution of pH after the wet oxidation treatment is shown Figure 9. The initial pH of the synthetic water was 7.5, since, as it was commented in material and methods section, this value was adjusted with sulphuric acid. It worthy to note that the pH rapidly increased to 12–13 in all experiments in catalysts were added. This is due to the presence of $\text{Ca}(\text{OH})_2$ in their composition, as it was proved by XRD and FTIR analyses, which is a strong base [56] that caused the increase in pH. This high amount of $\text{Ca}(\text{OH})_2$ is originated from the hydration of the calcium oxide, which is the main component of the waste eggshell after strong calcination [21].

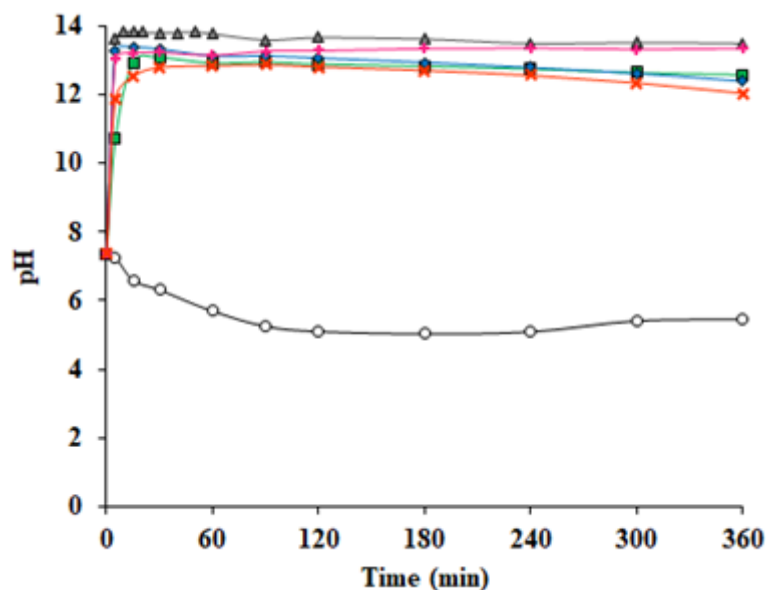


Figure 9. Evolution of pH with time in absence of catalyst (○), and in presence of the eggshell (▲) and the supported catalysts: Fe 5% (+), Fe 15% (×), Cu 5% (■), and Cu 15% (◆). In all cases, $T = 150\text{ }^{\circ}\text{C}$, $P = 40\text{ bar}$, $\text{pH} = 7.5$, initial HA concentration = 400 ppm and catalyst concentration = 1 g/L.

On the contrary, in the experiments without catalyst, pH values decreased to 5.4 after 6 h of treatment. Mahvi et al. [43] also found that the pH of the initial solution of humic substances in water decreased slightly during different treatment processes. Humic acids are weak acidic electrolytes with carboxylic- and phenolic-OH groups with a micelle-like structure. When HA in aqueous solution are thermally treated with temperatures above $70\text{ }^{\circ}\text{C}$, they formed more condensed polyaromatic structures, whereas at higher temperatures ($>110\text{ }^{\circ}\text{C}$), gradual decomposition resulting in the formation of carbon dioxide takes place [57]. These changes are responsible for the pH modification of synthetic water observed during WO treatment.

4. Conclusions

Eggshell can be used as support for the synthesis of heterogeneous catalysts to be used in the catalytic wet oxidation of humic acid. Five different materials were obtained: calcined eggshell, iron, or copper (5%wt.) supported on calcined eggshell and iron or copper (15%wt.) supported on calcined eggshell. These materials are essentially macroporous, the BET areas ranging from 4 to $6\text{ m}^2/\text{g}$. Besides, they are thermally stable up to $450\text{ }^{\circ}\text{C}$, thus being ideal catalysts to be employed in WO tests. The use of iron or copper supported catalysts improved significantly COD removal, the values varying from 62.8% to 82.3%, after 6 h of WO, whereas in absence of catalyst, only 8.8% removal was obtained. The best results were obtained with copper (15%wt.) supported on calcined eggshell, achieving a COD removal of 74.1% after 3 h of WO. This can be explained considering the higher metal loading and the good metal distribution on the surface of the support, based on HAADF-STEM micrographs.

Finally, it should be pointed out that calcined eggshell without metals can also be considered an interesting material to degrade HA. Although the removal of COD is moderate, a highly biodegradable effluent ($\text{BOD}_5/\text{COD} = 0.73$) was attained. This is an important issue, since metal catalysts may cause secondary pollution, although base metals, such as iron and copper, are considered to be metals with minimal safety concerns. Additionally, the use of metals implies economical costs.

Thus, further research on the possible applications of the calcined eggshell and copper-supported materials as catalysts in WO treatments can be a topic of great interest, in order to widen the knowledge about the optimum WO conditions, degradation degree of real wastewaters polluted with refractory compounds, catalyst reuse and oxidation mechanisms.

Supplementary Materials: The following are available online at <http://www.mdpi.com/2073-4441/12/1/100/s1>, Table S1. Instrumental parameters for ICP-MS; Table S2. Textural properties of the calcined eggshell and the iron and copper supported catalysts determined by N₂ adsorption-desorption at 77 K; Table S3. Concentration of iron and copper in the aqueous solutions after the WO treatment of HA solution; Table S4. Chemical composition in weight percentage of the used catalysts measured by XRF; Figure S1. Nitrogen adsorption-desorption isotherms at 77 K: (a) calcined eggshell, (b) Fe 5%, (c) Fe 15%, (d) Cu 5%, and (e) Cu 15%; Figure S2. Evolution of COD concentration with time in presence of pure CaO at pH 12 (spotted area) and at pH 7.5 (horizontal lines). In all cases, T = 150 °C, P = 40 bar, initial COD concentration = 367 ppm and catalyst concentration = 1 g/L; Figure S3. HAADF-STEM micrograph of Fe 5% and the elemental mapping of O, Mg, Ca and Fe; Figure S4. HAADF-STEM micrograph of Fe 15% and the elemental mapping of O, Mg, Ca and Fe; Figure S5. HAADF-STEM micrographs of Cu 5% and the elemental mapping of O, Mg, Ca and Cu; Figure S6. HAADF-STEM micrographs of Cu 15% and the elemental mapping of O, Mg, Ca and Cu.

Author Contributions: The individual contribution of each of the authors is the following: conceptualization, M.D.; methodology, P.O. and A.L.; validation, P.O. and A.L.; formal analysis, P.O. and A.L.; investigation, S.C.; resources, M.D.; data curation, M.D.; writing—original draft preparation, P.O. and A.L.; writing—review and editing, P.O. and A.L.; visualization, P.O. and S.C.; supervision, M.D.; project administration, M.D.; funding acquisition, M.D. All authors have read and agreed to the published version of the manuscript.

Funding: This research was funded by the Employment, Industry and Tourism Office of Principality of Asturias (Spain), grant number “IDI/2018/000127”.

Acknowledgments: Authors want to acknowledge the Scientific and Technical Services of the University of Oviedo for their support in the characterization of the samples.

Conflicts of Interest: The authors declare no conflict of interest.

References

1. Han, J.-L.; Xia, X.; Haider, M.R.; Jiang, W.-L.; Tao, Y.; Liu, M.-J.; Wang, H.-c.; Ding, Y.-C.; Hou, Y.-N.; Cheng, H.-Y.; et al. Functional graphene oxide membrane preparation for organics/inorganic salts mixture separation aiming at advanced treatment of refractory wastewater. *Sci. Total Environ.* **2018**, *628*, 261–270. [[CrossRef](#)] [[PubMed](#)]
2. Mylapilli, S.V.P.; Reddy, S.N. Sub and supercritical water oxidation of pharmaceutical wastewater. *J. Environ. Chem. Eng.* **2019**, *7*, 103165. [[CrossRef](#)]
3. Luan, M.; Jing, G.; Piao, Y.; Liu, D.; Jin, L. Treatment of refractory organic pollutants in industrial wastewater by wet air oxidation. *Arab. J. Chem.* **2017**, *10*, S769–S776. [[CrossRef](#)]
4. Manjari, S.; Meenal, G.; Sushil, K.A.; Pawan, D. Removal of Refractory Organic Compounds from Wastewater by Various Advanced Oxidation Process—A Review. *Curr. Environ. Eng.* **2019**, *6*, 8–16. [[CrossRef](#)]
5. Li, J.; Hao, X.; van Loosdrecht, M.C.M.; Yu, J.; Liu, R. Adaptation of semi-continuous anaerobic sludge digestion to humic acids. *Water Res.* **2019**, *161*, 329–334. [[CrossRef](#)]
6. Liu, X.; Zhang, M.; Li, Z.; Zhang, C.; Wan, C.; Zhang, Y.; Lee, D.-J. Inhibition of urease activity by humic acid extracted from sludge fermentation liquid. *Bioresour. Technol.* **2019**, *290*, 121767. [[CrossRef](#)]
7. Li, X.Z.; Li, F.B.; Fan, C.M.; Sun, Y.P. Photoelectrocatalytic degradation of humic acid in aqueous solution using a Ti/TiO₂ mesh photoelectrode. *Water Res.* **2002**, *36*, 2215–2224. [[CrossRef](#)]
8. Oulego, P.; Collado, S.; Laca, A.; Díaz, M. Impact of leachate composition on the advanced oxidation treatment. *Water Res.* **2016**, *88*, 389–402. [[CrossRef](#)]
9. Jiang, F.; Qiu, B.; Sun, D. Degradation of refractory organics from biologically treated incineration leachate by VUV/O₃. *Chem. Eng. J.* **2019**, *370*, 346–353. [[CrossRef](#)]
10. Delgado, J.J.; Pérez-Omil, J.A.; Rodríguez-Izquierdo, J.M.; Cauqui, M.A. The role of the carbonaceous deposits in the Catalytic Wet Oxidation (CWO) of phenol. *Catal. Commun.* **2006**, *7*, 639–643. [[CrossRef](#)]
11. Mohite, R.G.; Garg, A. Performance of heterogeneous catalytic wet oxidation for the removal of phenolic compounds: Catalyst characterization and effect of pH, temperature, metal leaching and non-oxidative hydrothermal reaction. *J. Environ. Chem. Eng.* **2017**, *5*, 468–478. [[CrossRef](#)]
12. Bhargava, S.K.; Tardio, J.; Prasad, J.; Föger, K.; Akolekar, D.B.; Grocott, S.C. Wet Oxidation and Catalytic Wet Oxidation. *Ind. Eng. Chem. Res.* **2006**, *45*, 1221–1258. [[CrossRef](#)]
13. Heponiemi, A.; Azalim, S.; Hu, T.; Lassi, U. Cerium Oxide Based Catalysts for Wet Air Oxidation of Bisphenol A. *Top. Catal.* **2015**, *58*, 1043–1052. [[CrossRef](#)]
14. Santhosh, C.; Velmurugan, V.; Jacob, G.; Jeong, S.K.; Grace, A.N.; Bhatnagar, A. Role of nanomaterials in water treatment applications: A review. *Chem. Eng. J.* **2016**, *306*, 1116–1137. [[CrossRef](#)]

15. Zhao, W.; Chen, I.W.; Huang, F. Toward large-scale water treatment using nanomaterials. *Nano Today* **2019**, *27*, 11–27. [[CrossRef](#)]
16. Martins, R.; Domingues, E.; Bosio, M.; Quina, M.; Gmurek, M.; Quinta-Ferreira, R.; Gomes, J. Effect of Different Radiation Sources and Noble Metal Doped onto TiO₂ for Contaminants of Emerging Concern Removal. *Water* **2019**, *11*, 894. [[CrossRef](#)]
17. Nasrollahzadeh, M.; Sajadi, S.M.; Hatamifard, A. Waste chicken eggshell as a natural valuable resource and environmentally benign support for biosynthesis of catalytically active Cu/eggshell, Fe₃O₄/eggshell and Cu/Fe₃O₄/eggshell nanocomposites. *Appl. Catal. B Environ.* **2016**, *191*, 209–227. [[CrossRef](#)]
18. Chua, S.Y.; Periasamy, L.A.P.; Goh, C.M.H.; Tan, Y.H.; Mubarak, N.M.; Kansedo, J.; Khalid, M.; Walvekar, R.; Abdullah, E.C. Biodiesel synthesis using natural solid catalyst derived from biomass waste—A review. *J. Ind. Eng. Chem.* **2020**, *81*, 41–60. [[CrossRef](#)]
19. Nath, B.; Kalita, P.; Das, B.; Basumatary, S. Highly efficient renewable heterogeneous base catalyst derived from waste Sesamum indicum plant for synthesis of biodiesel. *Renew. Energy* **2019**. [[CrossRef](#)]
20. Chenrayan, S.; VEDIAPPAN, K.; Murugan, N.; Kang, H.; Santhoshkumar, P.; Gnanamuthu, R.M.; Lee, C. Thermochemical Conversion of Eggshell as Biological Waste and its Application as a Functional Material for Lithium-ion Batteries. *Chem. Eng. J.* **2019**, 372. [[CrossRef](#)]
21. Laca, A.; Laca, A.; Díaz, M. Eggshell waste as catalyst: A review. *J. Environ. Manag.* **2017**, *197*, 351–359. [[CrossRef](#)] [[PubMed](#)]
22. Hossain, S.S.; Roy, P.K. Development of waste derived nano-lakargiite bonded high alumina refractory castable for high temperature applications. *Ceram. Int.* **2019**, *45*, 16202–16213. [[CrossRef](#)]
23. Karoshi, G.; Kolar, P.; Shah, S.B.; Gilleskie, G. Valorization of Eggshell Waste into Supported Copper Catalysts for Partial Oxidation of Methane. *Int. J. Environ. Res.* **2019**. [[CrossRef](#)]
24. Sajadi, S.M.; Kolo, K.; Abdullah, S.M.; Hamad, S.M.; Khalid, H.S.; Yassein, A.T. Green synthesis of highly recyclable CuO/eggshell nanocomposite to efficient removal of aromatic containing compounds and reduction of 4-nitrophenol at room temperature. *Surf. Interfaces* **2018**, *13*, 205–215. [[CrossRef](#)]
25. Sietsma, J.R.A.; Jos van Dillen, A.; de Jongh, P.E.; de Jong, K.P. Application of ordered mesoporous materials as model supports to study catalyst preparation by impregnation and drying. In *Studies in Surface Science and Catalysis*; Gaigneaux, E.M., Devillers, M., De Vos, D.E., Hermans, S., Jacobs, P.A., Martens, J.A., Ruiz, P., Eds.; Elsevier: Amsterdam, The Netherlands, 2006; Volume 162, pp. 95–102.
26. Degen, T.; Sadki, M.; Bron, E.; König, U.; Nénert, G. The HighScore suite. *Powder Diffr.* **2014**, *29*, S13–S18. [[CrossRef](#)]
27. Barrett, E.P.; Joyner, L.G.; Halenda, P.P. The Determination of Pore Volume and Area Distributions in Porous Substances. I. Computations from Nitrogen Isotherms. *J. Am. Chem. Soc.* **1951**, *73*, 373–380. [[CrossRef](#)]
28. Oulego, P.; Collado, S.; Laca, A.; Díaz, M. Tertiary treatment of biologically pre-treated landfill leachates by non-catalytic wet oxidation. *Chem. Eng. J.* **2015**, *273*, 647–655. [[CrossRef](#)]
29. Mahvi, A.; Maleki, A.; Rezaee, R.; Safari, M. Reduction of humic substances in water by application of ultrasound waves and ultraviolet irradiation. *Iran. J. Environ. Health Sci. Eng.* **2009**, *6*, 233–240.
30. Fernandes, A.; Santos, D.; Pacheco, M.J.; Ciríaco, L.; Lopes, A. Electrochemical oxidation of humic acid and sanitary landfill leachate: Influence of anode material, chloride concentration and current density. *Sci. Total Environ.* **2016**, *541*, 282–291. [[CrossRef](#)]
31. APHA; AWWA; WEF. *Standard Methods for Examination of Water and Wastewater*, 20th ed.; APHA, AWWA, WEF, Eds.; APHA: Washington, DC, USA, 1999.
32. Yaşar, F. Biodiesel production via waste eggshell as a low-cost heterogeneous catalyst: Its effects on some critical fuel properties and comparison with CaO. *Fuel* **2019**, *255*, 115828. [[CrossRef](#)]
33. Goli, J.; Sahu, O. Development of heterogeneous alkali catalyst from waste chicken eggshell for biodiesel production. *Renew. Energy* **2018**, *128*, 142–154. [[CrossRef](#)]
34. Habte, L.; Shiferaw, N.; Mulatu, D.; Thenepalli, T.; Chilakala, R.; Ahn, J.W. Synthesis of Nano-Calcium Oxide from Waste Eggshell by Sol-Gel Method. *Sustainability* **2019**, *11*, 3196. [[CrossRef](#)]
35. Alvarez-Torrellas, S.; Boutahala, M.; Boukhalfa, N.; Munoz, M. Effective Adsorption of Methylene Blue dye onto Magnetic Nanocomposites. Modeling and Reuse Studies. *Appl. Sci.* **2019**, *9*, 4563. [[CrossRef](#)]
36. El-Trass, A.; ElShamy, H.; El-Mehasseb, I.; El-Kemary, M. CuO nanoparticles: Synthesis, characterization, optical properties and interaction with amino acids. *Appl. Surf. Sci.* **2012**, *258*, 2997–3001. [[CrossRef](#)]

37. Ren, F.; Ding, Y.; Leng, Y. Infrared spectroscopic characterization of carbonated apatite: A combined experimental and computational study. *J. Biomed. Mater. Res. Part A* **2014**, *102*, 496–505. [[CrossRef](#)]
38. Mosaddegh, E. Ultrasonic-assisted preparation of nano eggshell powder: A novel catalyst in green and high efficient synthesis of 2-aminochromenes. *Ultrason. Sonochem.* **2013**, *20*, 1436–1441. [[CrossRef](#)]
39. Golmohammad, M.; Golestanifard, F.; Mirhabibi, A. Synthesis and Characterization of Maghemite as an Anode for Lithium-Ion Batteries. *Int. J. Electrochem. Sci.* **2016**, *11*, 6432–6442. [[CrossRef](#)]
40. Witoon, T. Characterization of calcium oxide derived from waste eggshell and its application as CO₂ sorbent. *Ceram. Int.* **2011**, *37*, 3291–3298. [[CrossRef](#)]
41. Doostmohammadi, A.; Monshi, A.; Salehi, R.; Fathi, M.H.; Golniya, Z.; Daniels, A.U. Bioactive glass nanoparticles with negative zeta potential. *Ceram. Int.* **2011**, *37*, 2311–2316. [[CrossRef](#)]
42. Nazari, M.; Ghasemi, N.; Maddah, H.; Motlagh, M.M. Synthesis and characterization of maghemite nanopowders by chemical precipitation method. *J. Nanostruct. Chem.* **2014**, *4*, 99. [[CrossRef](#)]
43. Galván-Ruiz, M.; Hernández, J.; Baños, L.; Noriega-Montes, J.; Rodríguez-García, M.E. Characterization of Calcium Carbonate, Calcium Oxide, and Calcium Hydroxide as Starting Point to the Improvement of Lime for Their Use in Construction. *J. Mater. Civ. Eng.* **2009**, *21*, 694–698. [[CrossRef](#)]
44. Ethiraj, A.S.; Kang, D.J. Synthesis and characterization of CuO nanowires by a simple wet chemical method. *Nanoscale Res. Lett.* **2012**, *7*, 70. [[CrossRef](#)] [[PubMed](#)]
45. Rouquerol, F.; Rouquerol, J.; Sing, K.S.W.; Maurin, G.; Llewellyn, P. 1—Introduction. In *Adsorption by Powders and Porous Solids*, 2nd ed.; Rouquerol, F., Rouquerol, J., Sing, K.S.W., Llewellyn, P., Maurin, G., Eds.; Academic Press: Oxford, UK, 2014; pp. 1–24. [[CrossRef](#)]
46. Gao, Y.; Xu, C. Synthesis of dimethyl carbonate over waste eggshell catalyst. *Catal. Today* **2012**, *190*, 107–111. [[CrossRef](#)]
47. Kim, T.; Olek, J. Effects of Sample Preparation and Interpretation of Thermogravimetric Curves on Calcium Hydroxide in Hydrated Pastes and Mortars. *Transp. Res. Rec. J. Transp. Res. Board* **2012**, *2290*, 10–18. [[CrossRef](#)]
48. Keely, W.M.; Maynor, H.W. Thermal Studies of Nickel, Cobalt, Iron and Copper Oxides and Nitrates. *J. Chem. Eng. Data* **1963**, *8*, 297–300. [[CrossRef](#)]
49. Li, X.-G.; Lv, Y.; Ma, B.-G.; Wang, W.-Q.; Jian, S.-W. Decomposition kinetic characteristics of calcium carbonate containing organic acids by TGA. *Arab. J. Chem.* **2017**, *10*, S2534–S2538. [[CrossRef](#)]
50. Wang, P.; Zeng, G.; Peng, Y.; Liu, F.; Zhang, C.; Huang, B.; Zhong, Y.; He, Y.; Lai, M. 2,4,6-Trichlorophenol-promoted catalytic wet oxidation of humic substances and stabilized landfill leachate. *Chem. Eng. J.* **2014**, *247*, 216–222. [[CrossRef](#)]
51. Hajimirzaee, S.; Soleimani Mehr, A.; Ghavipour, M.; Vatankhah, M.; Behbahani, R.M. Effect of metal loading on catalytic activity and selectivity of ZSM-5 zeolite catalyst in conversion of methanol to olefins and aromatics. *Pet. Sci. Technol.* **2017**, *35*, 279–286. [[CrossRef](#)]
52. Urrea, J.L.; García, M.; Collado, S.; Oulego, P.; Díaz, M. Sludge hydrothermal treatments. Oxidising atmosphere effects on biopolymers and physical properties. *J. Environ. Manag.* **2018**, *206*, 284–290. [[CrossRef](#)]
53. Fukushima, M.; Tatsumi, K.; Nagao, S. Degradation Characteristics of Humic Acid during Photo-Fenton Processes. *Environ. Sci. Technol.* **2001**, *35*, 3683–3690. [[CrossRef](#)]
54. Da, X.; Ji, H.; Zhao, Z.; Lan, R.; Li, T.; Ma, J. Strongly prolonged hydroxyl radical production for Fenton-like reactions: The golden touch of Cu. *Sep. Purif. Technol.* **2019**, *213*, 500–506. [[CrossRef](#)]
55. Miao, X.; Dai, H.; Chen, J.; Zhu, J. The enhanced method of hydroxyl radical generation in the heterogeneous UV-Fenton system with α -FeOOH as catalyst. *Sep. Purif. Technol.* **2018**, *200*, 36–43. [[CrossRef](#)]
56. Cavalcante, A.d.M.; Lima, J.C.d.S.; Santos, L.d.M.; Oliveira, P.C.C.d.; Ribeiro Júnior, K.A.L.; Sant'ana, A.E.G. Comparative evaluation of the pH of calcium hydroxide powder in contact with carbon dioxide (CO₂). *Mater. Res.* **2010**, *13*, 1–4. [[CrossRef](#)]
57. Kolokassidou, C.; Pashalidis, I.; Costa, C.N.; Efstathiou, A.M.; Buckau, G. Thermal stability of solid and aqueous solutions of humic acid. *Thermochim. Acta* **2007**, *454*, 78–83. [[CrossRef](#)]

